DUMAS Jonathan

Design of a High Intensity Positron Source

Internship report
Under the direction of Eric Voutier

June 2007

M2 of Instrumentation Physics

TABLE OF CONTENTS

Thanks

I would like to thank all the people who have been helping me in this internship:

I would like to thank my advisor, Eric Voutier, always available for questions and remarks and trusting me to do this work.

Jean-Sébastien Réal for sharing his computing skills, all the crew I have been working with, Javier Rodrigez Vignote, Pascal Carrivain, Christophe Furget, Serge Kox, Jean Mougey, Maud Versteegen.

I would like to thank Serkan Golge at JLab for his explanations and François Méot for his advices.

1. INTRODUCTION

The production of high intensity (un)polarized positron beams is an important concern of the accelerator physics community: very high energy positrons are an elementary brick of the ILC (International Linear Collider) project [1]; the operation of high energy positrons at HERA will soon finish, and might become an opportunity for the CEBAF accelerator [2]; low energy positrons are also expected to participate to anti-matter research, in building anti-hydrogen atoms from anti-protons and positrons [3]; at very low energy, positrons can also be used for the study of the structure of a material [4]. The aim of this report is to address several questions about the feasibility of a positron beam, in the context of the Jefferson Laboratory (JLab) accelerator system.

There are essentially two ways of commonly producing positrons: the β^+ decay, and the pair production from a photon source. The former corresponds to the disintegration $p \rightarrow n + e^+ + \nu_e$ of a proton of a nuclear media, for example the sodium isotope ^{22}Na; this type of radioactive source is compact and widely used in laboratories, but its mean lifetime is unfortunately short (2.6 years), and intensities are limited. Pair production is the most widely used mechanism for producing e^+ at facilities having relativistic electrons: SLAC (Stanford Linear Accelerator Center) with a 3.1 GeV/c pulsed positron beam [5], KEK (Tsukuba High Energy Physics Laboratory) with a 3.5 GeV/c pulsed positron beam [6], LLNL (Lawrence Livermore National Laboratory) producing positrons with a 100 MeV/c and 300 μA pulsed electron beam [7]. This work presents the preliminary studies on a pair production based positron source.

The final constraints, which make this design completely original, are the delivering of a continuous 100 nA positron beam to experimental areas for physics studies at 11 GeV/c. Such a beam would definitely contribute to the study of the partonic structure of the nucleon, one of the leading topic of the JLab 12 GeV upgrade [8].

We first discuss the advantage of positron beams for the study of different physics fields, including nuclear physics with Deeply Virtual Compton Scattering (DVCS) experiments, and material science with Positron Annihilation Spectroscopy. The basic mechanisms for the production of positrons on a target are then presented and the GEANT4 simulator, elaborated during the present training period, is discussed. On the basis of this simulator, the study of the main parameters governing positron production is performed and compared to earlier studies at different laboratories. Finally, a global scheme of the project is presented.

2. PHYSICS MOTIVATIONS

2.1. Deeply virtual Compton scattering

Similarly to the diffusion of light by a material, Deeply Virtual Compton Scattering (DVCS) corresponds to the scattering of a virtual photon by a quark. The purpose of these experiments is the study of the inner structure of the nucleon, the distribution and the dynamics of the quark and gluon content, which can be accessed through the measurement of Generalized Parton Distributions (GPDs).

GPDs are a set of mathematical functions which describe the non-trivial internal structure of nucleons. They correspond to the overlap probability of picking a quark inside the nucleon and putting it back with different (or same) spin and momentum. These functions can be used to locate the quarks and gluons inside nucleons: GPDs can be interpreted in an impact parameter space as the distribution, in the plane transverse to motion, of the quarks carrying a given longitudinal momentum (Fig. 1).
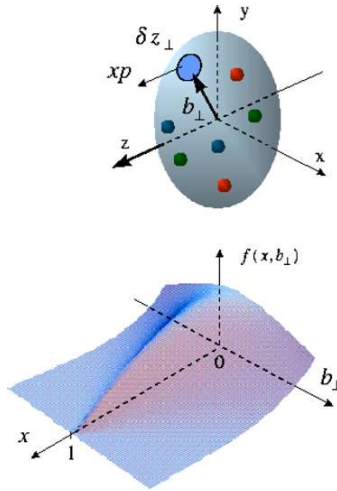

Figure 1: Representation of a GPD in an impact parameter space [9].

The GPDs can be accessed in exclusive inelastic reactions in the Bjorken regime, that is in a kinematical regime where the wavelength of the virtual photon is smaller than the nucleon size. The simplest reaction is a collision where a lepton strikes a quark inside the nucleon. The virtual photon exchanged in this collision is absorbed by the quark that emits quasi-instantaneously a real photon (or a neutral meson in deeply virtual meson production). This is the scheme of the DVCS reaction. The GPDS appear in the reaction amplitude:

$$\tau_{DVCS} \propto \int dx \left[\frac{1}{x - \xi + i\delta} - \frac{1}{x + \xi - i\delta} \right] GPD(x, \xi, t) \tag{1}$$

where -2ξ is the fraction of the transferred longitudinal momentum to the quark by the virtual photon, and *t* is the momentum transfer to the nucleon. The electro-production of photons gets contributions from two indistinguishable mechanisms: the DVCS process, and the Bethe-
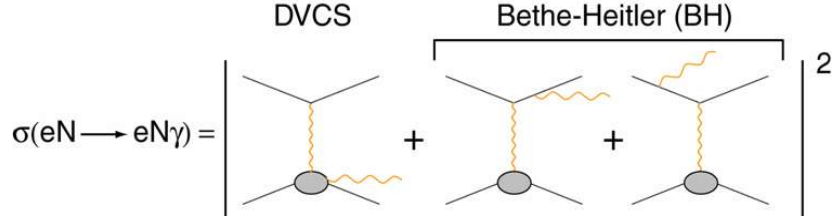

Figure 2: The different contributions to electro-production of photons.

Heitler (BH) process where the real photon is emitted either by the incoming or scattered electron (Fig. 2). The cross section for the global process is the coherent sum of each amplitude:

$$\frac{d^5\sigma}{d\Omega^5} = \tau^2_{BH} + |\tau_{DVCS}|^2 + 2\ \tau_{BH}\ \Re e\left\{\tau_{DVCS}\right\} \tag{2}$$

where the last term on the right-hand side is the contribution from the interference between the BH and DVCS amplitude. The BH process is however well known and exactly calculable from the electromagnetic form factors of the nucleon. In the 6-11 GeV/*c* energy range of JLab, the cross section gets significant contributions from the BH process: DVCS appears only as deviations from the large BH contribution. In addition the cross section figures a bilinear form of the DVCS amplitude, difficult to separate from the interference contribution, which leads to more ambiguous interpretation in terms of GPDs. This problem is resolved by considering the sensitivity of the global process to the lepton beam polarization and charge. Measuring the helicity dependent cross section difference:

$$\frac{d^5\dot{\sigma}}{d\Omega^5} - \frac{d^5\sigma}{d\Omega^5} = 2\ \tau_{BH}\ \Im m\left\{\tau_{DVCS}\right\} + 2\ \Re e\left\{\tau_{DVCS}\right\}\ \Im m\left\{\tau_{DVCS}\right\} \tag{3}$$

one can extract the imaginary part of the DVCS amplitude, considering that the second part on the right-hand side of the previous relation is negligible. However, measuring the charge dependent cross section, one access the cross section difference:

$$\frac{d^5\sigma^+}{d\Omega^5} - \frac{d^5\sigma^-}{d\Omega^5} = 4\ \tau_{BH}\ \Re e\left\{\tau_{DVCS}\right\} \tag{4}$$

which appears as a pure DVCS signal isolating the real part of the reaction amplitude. Therefore, within the DVCS context, the availability of an accelerated positron beam is providing a new and clean observable of the nucleon structure.

2.2. Positron annihilation spectroscopy

The lifetime of a positron inside a solid is very short (~hundreds of picoseconds) but is long enough to enable the positron to visit a region of a material, and to sense the atomic and electronic structure of the environment. Therefore, positrons can be used as accelerator as a

probe of the atomic structure. Positron spectroscopy applications are extending from advanced problems of solid-state physics to industrial application in the field of high-technology materials, and from the study of metals and alloys to polymers and semiconductors. More accurately, the positrons annihilation spectroscopy (PAS) is nowadays known as a powerful to investigate the microstructure of condensed matter.

Injecting a positron in a sample allows to get information about the microscopic properties of a material. Basically, the principles of PAS can be summarised as:

    i)   A positron is injected in a material, gets quickly in thermal equilibrium with the surroundings, and interacts with the environment.

    ii)   The positron annihilates with an electron of the medium. The structure of the medium is characterized by the measurement of the parameters of the annihilation reaction. For a homogeneous material without defects, all positrons would annihilate within the same lifetime τ , specific of the material.
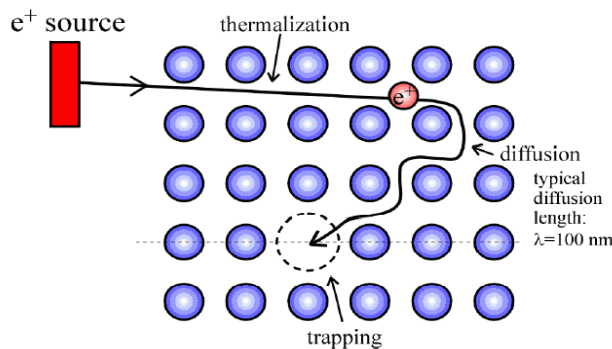

Figure 3: Positron trapping in a defect [10].

The positrons are preferably moving in the inter-atomic space, repelled by the Coulomb force of positive core atoms. When a defect occurs, positrons might see a lower Coulomb repulsion either because of a missing atom (Fig. 3) or a dislocation; positrons can be trapped in these there until it annihilation.
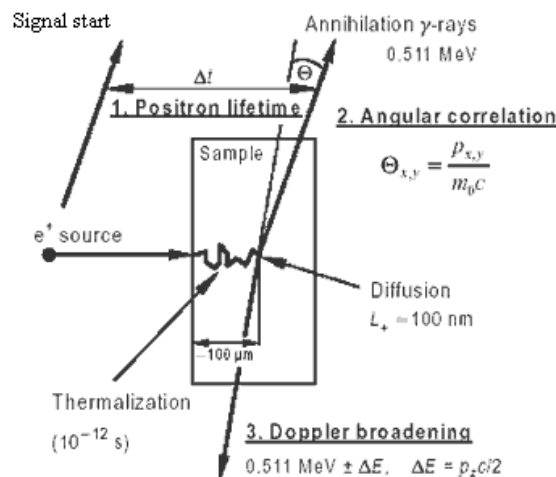

Figure 4: Example of PAS techniques [10].

PAS gives essentially two parameters characterizing the medium structure: a first quantity related to the positron state (free, captured in a trap, bound in a positronium atom…), and depending on its history in the material; a second quantity which gives information about the electron involved in the annihilation reaction, namely, the electronic structure of the local annihilation site. Several experimental techniques can be used (Fig. 4). Two of them are described in the following.

2.2.1. Positron lifetime spectroscopy

Positron annihilation lifetime spectroscopy (PALS) is a very efficient method to density and size defects. A pulsed positron beam that delivers a START signal for time measurement, is usually used for PALS. The START signal is generated by a positron bunch which duration has to be of the order of 100 ps. The time difference between the instant a positron enters the material (START) and the moment the radiation due to positron annihilation is detected (STOP) is measured. Spectra of positron lifetimes as an histogram of counts $N(t)$ are obtained. They are composed from a sum of exponential components

$$N(t) = \sum_{i=1}^{n} \frac{I_i}{\tau_i} \exp\left(-\frac{t}{\tau_i}\right) \tag{5}$$

where τ_i are the positron lifetimes (Tab. 1), and I_i are the corresponding positron fractions. The number of components n is equal to the number of different states from which the positron can annihilate. In the case of k types of defect, $n=k+1$; if no defect,

$$N(t) = \frac{1}{\tau} \exp\left(-\frac{t}{\tau}\right) \quad . \tag{6}$$

Positron State	Type of process	Characteristic lifetime depending on the material
free positron	2 gammas	0.1-0.4 ns
Trapped positron	2 gammas	0.2-0.5 ns
para-Ps	2 gammas, self-annihilation	0.1 ns
	2 gammas, pick-off process	>1 ns
ortho-Ps	3 gammas, self-annihilation	140 ns
	2 gammas, pick-off process	>1 ns

Table 1: Characteristic lifetimes of positrons in different states [11].

Positron decay spectra are recorded as a function of time. Figure 5a highlights two decay constants corresponding to different lifetimes. A short lifetime indicate the decay of free

positrons while it takes a longer time for positrons trapped in defects because of lower electron densities. Figure 5b also shows that the decay spectrum of a pure material like as-grown Czochralski silicon is different from a plastically deformed silicon: one lifetime only is found for the pure material (τ_b=218 ps), and three for the plastically deformed silicon with (τ_1=120 ps, τ_2=320 ps and τ_3=520 ns).
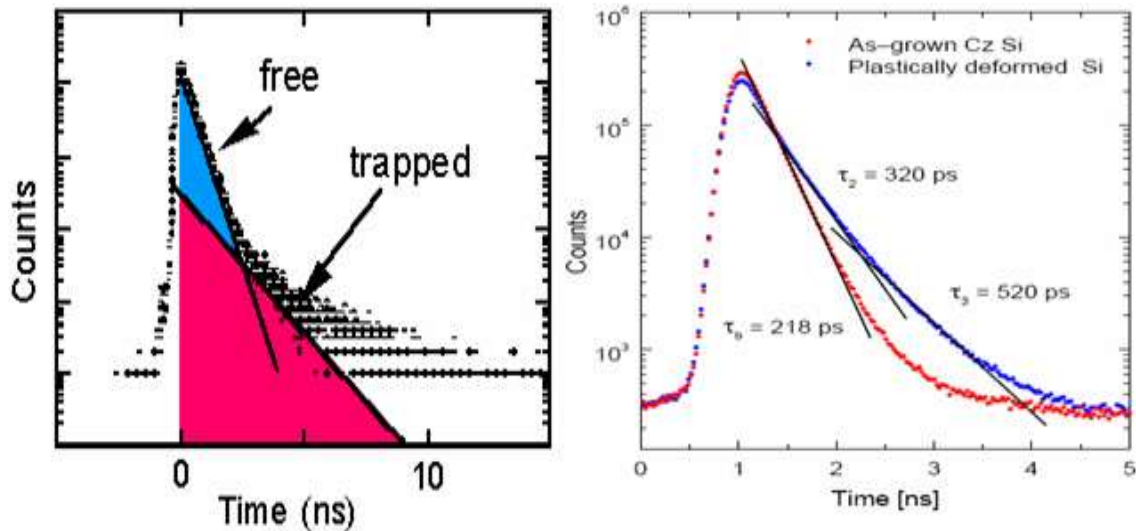

Figure 5a [12] and 5b [10]: Positrons lifetime spectra.

2.2.2. Doppler broadening

Another technique is based on the principle of momentum conservation in the annihilation process of the e^-e^+ pair. The electron motion in the propagation direction (p_z) of the photons is causing a Doppler Broadening of the Annihilation Line (DBAL). A Doppler shift ΔE from the characteristic 511 keV photons can be measured with an energy dispersive detector system (Fig. 6) having a good energy resolution (1.2 to 2.2 keV).
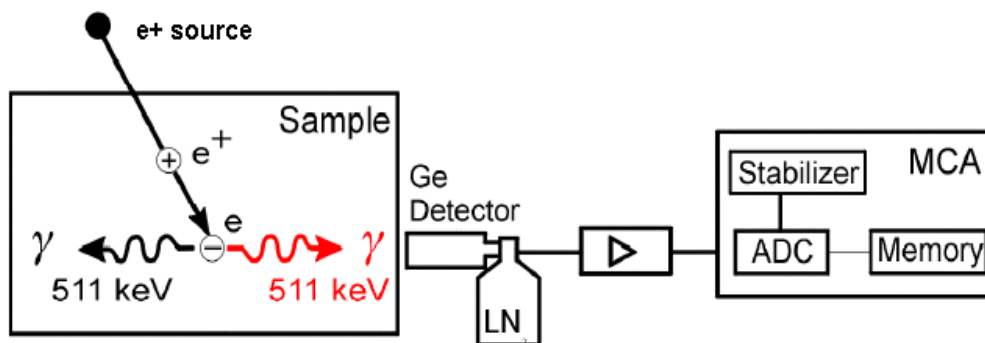

Figure 6: Doppler Broadening setup [10].

The Doppler shift is related to the electron momentum component via the relation:

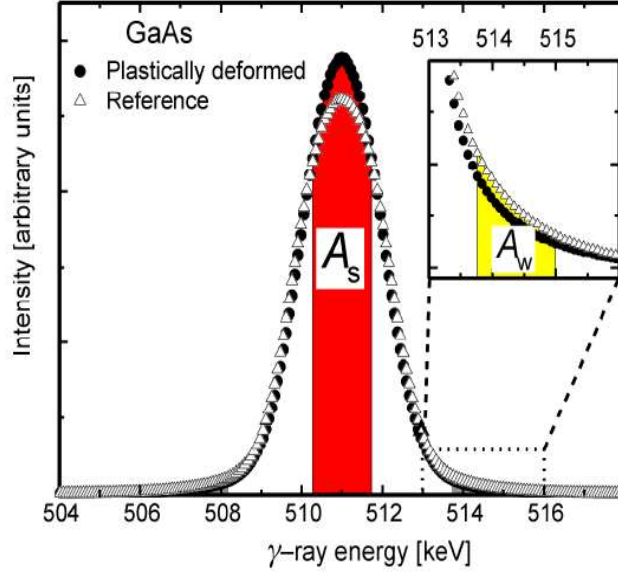$$\Delta E = \frac{p_z c}{2} \tag{7}$$

9

Figure 7: Photon energy spectrum produced in a Zinc-dopped Gallium without defect and in a plastically deformed GaAs [10].

In practice, an energy spectrum of produced photons is measured: in Fig. 7, a lot of annihilation events are summed to get a Doppler-broadened spectrum of the 511 keV annihilation line. One can extract two parameters S and W defined as:

$$S = \frac{A_S}{A_0}$$

(8)

where A_S is the area of the low momentum part around 511 keV, A_W is the area determined at high momenta, and A_0 is the whole area. S and W are sensitive to the defect concentration: W is used to study the core electrons that have high momenta, leading to larger shift photon, and is related to the chemical surroundings of the annihilation site; the S parameter is probing the valence electrons, and is increasing in presence of an open-volume defect. For example, comparing the reference material to the deformed one (Fig. 7), the ratio $S_{deformed}$ / $S_{reference}$ is 1.0695 indicating a larger defects concentration.

3. Positron production fundamentals

Several physical effects have to be considered for the design of a positron source. A full view of the succession of events when a high celerity electron enters a material is shown below (Fig. 8), involving electrons, photons and positrons.
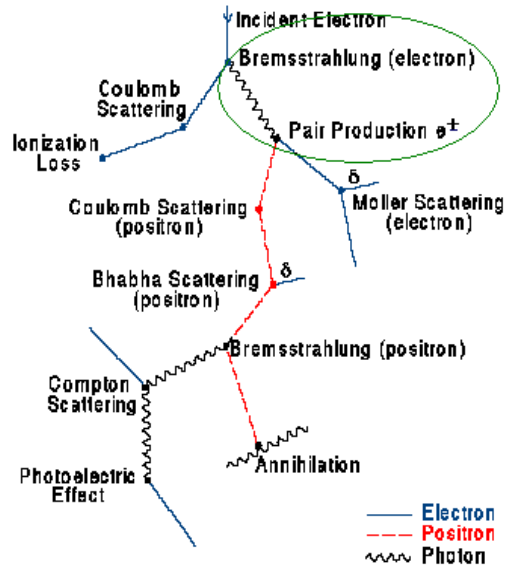

Figure 8: Full electromagnetic shower caused by an electron in a material [13].

An electron or a positron looses energy when travelling in a material. In the case of high Z material (for example lead in Fig. 9a), the main processes responsible for energy deposit are Bremsstrahlung and Ionization. The photons generated in the electromagnetic shower are interacting with matter essentially via the creation of $e^- e^+$ pairs above a few Mev (Fig. 9b).
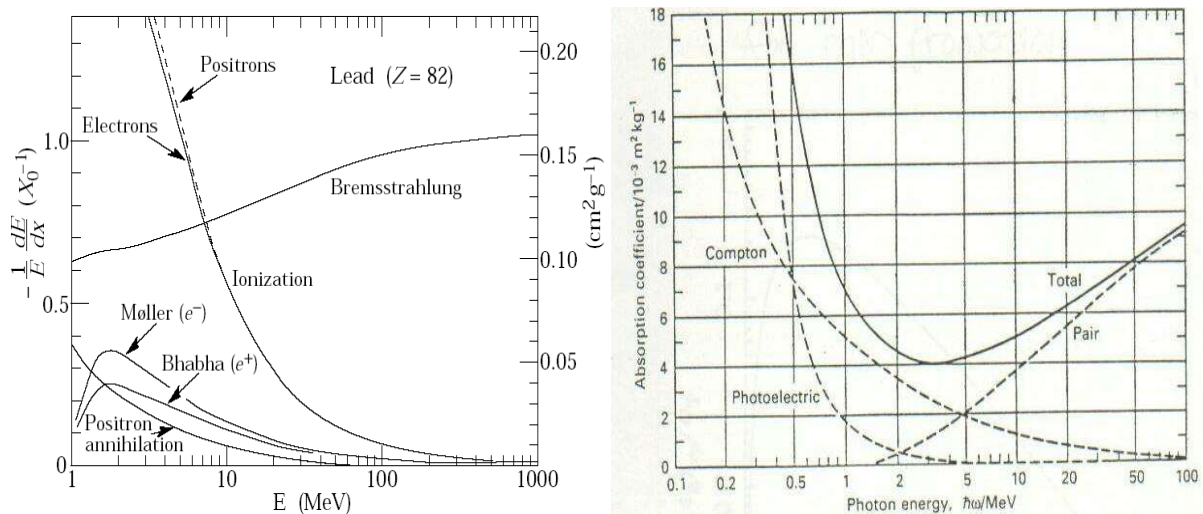

Figure 9a and b: Energy loss per radiation length in lead as a function of electron/positron energy [14]
and absorption coefficient for high energy photons in lead [15].

3.1. Bremsstrahlung

Positrons are generated by the photons radiated by the electrons following the Bremsstrahlung process. The braking or Bremsstrahlung radiation, is an electromagnetic radiation created by the deceleration of electric charges. When an electron hits a solid target, it is slowed down and deflected by the electric field of the atom's core of the target. According to Maxwell's equation, if a charged particle's celerity is changing, either its absolute value or its direction, the particle radiates energy (photons). This effect only becomes noticeable when the energy of the particle is very high compared to its mass, i.e. for relativistic particles.
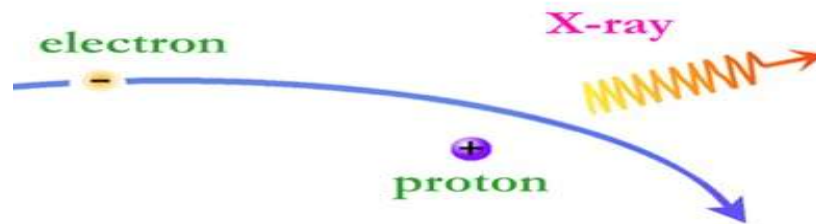

Figure 10: Photon emitted by Bremsstrahlung [16].

The mean energy loss by Bremsstrahlung as a function of the radiation length X_0 is increasing as E_0:

$$-\frac{dE}{dx} = \frac{E_0}{X_0} \quad .$$

(9)

The energy of the photons produced by Bremsstrahlung is depending on the energy levels of the atomic electrons, because free lepton motion and velocity is affected by the screening effect of the atomic electrons. As the deceleration of electrons is not quantized, it produces a photon flux with a continuous energy spectrum which maximum corresponds to the primary electron energy.

3.2. Pair creation

Finally, a pair of one electron and one positron is produced by the photon interacting with the Coulomb field of the nucleus of the atom.
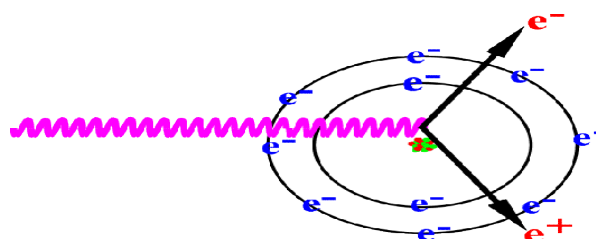

Figure 11: Electron-positron pair production [17].

The conservation of energy and momentum requires the photon to have a minimal energy $h\nu$ (h is Planck's constant and ν is the photon frequency) of twice the rest mass of an electron $2m_e c^2$ (1.022 MeV) in order to produce a pair. The photon cannot produce a pair in an empty space, and has to interact close to a nucleus. The extra energy of the photon is shared between the kinetic energy of the created pair and the recoil of the nucleus. Positrons and the electrons can be emitted at large angles, but statistically they move toward direction of the incoming photon.

Above a few MeV, pair production is the dominant mechanism for photon absorption in matter. The probability of a pair creation is increasing with the energy of the photon and with the Z of the material. The cross-section is given by :

$$\sigma_{\pi} = \alpha \, r_e^2 Z^2 \left[\frac{28}{9} \ln\left(\frac{2h\nu}{m_e c^2}\right) - \frac{218}{27} \right] \tag{10}$$

3.3. The electromagnetic cascade shower mechanism

An electromagnetic shower results from the succession of the previously described processes: an electron emits a Bremsstrahlung photon in a material, which subsequently produced a pair creation. The leptons can repeat this process as long as their energy is not dissipated via other mechanisms.

Important electromagnetic shower only occurs if the electrons injected in the material are more energetic than a critical energy E_c. The critical energy is not the energy below which an electromagnetic shower does not occur, but corresponds to the electron energy for which the average energy loss due to radiation equals the energy loss due to ionization. It is depending on the Z of the target according to

$$E_C(MeV) = \frac{610}{(Z+1.24)} \tag{11}$$

For example, the critical energy of Tungsten is E_c = 8.10 MeV.
An important characteristic of an electromagnetic shower is the radiation length X_0 which corresponds to the average distance of every generation of particles. It characterizes the amount of matter traversed by an electron which looses all its energy but 1/e via Bremsstrahlung, and is about 7/9 of the mean free path for pair production by a photon. The radiation length is given by, to a good approximation, by the expression:

$$X_0 = \frac{716.4\,g.cm^{-2}A}{Z(Z+1)\ln(287/\sqrt{Z})} \tag{12}$$

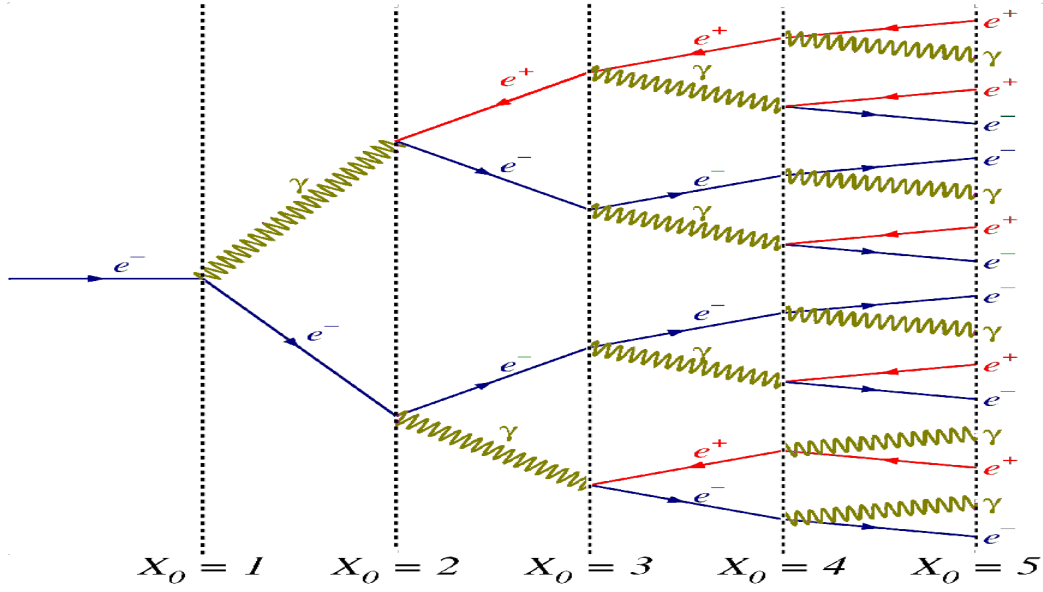For Tungsten, A = 184.84 uma and Z = 74 so X_0 = 3.6 mm.

Figure 12: Cascade shower mechanism [18].

The shower is strongly peaked in the forward direction. The typical angle of Bremsstrahlung photons and electrons and pair production is

$$\theta\ (rd) = \frac{m_e c^2}{E_0} \ . \tag{13}$$

3.4 Secondary mechanisms

At least four other processes turn out to be important for positron generation, regarding the power deposited in a target.

3.4.1 Ionization

Ionization is a major heating process. In this process, the incident particle transfers some of its kinetic energy to the medium. Part of it is transmitted to the atomic electrons that can be expulsed from atomic levels (δ rays in Fig. 8). In quantum field theory, this is called Møller scattering $e^- e^- \rightarrow e^- e^-$ for electrons and Bhabha scattering $e^+ e^- \rightarrow e^+ e^-$ for positrons. The energy lost by ionization follows the Bethe-Bloch formula:

$$-\frac{dE}{dx} = \frac{4\,\pi}{m_e c^2} N_A z^2 \frac{Z}{A} \cdot \frac{\rho}{\beta^2} \left(\frac{e^2}{4\,\pi\,\varepsilon_0} \right)^2 \cdot \left[\ln\left(\frac{2\,m_e c^2\,\beta^2}{I(1-\beta^2)} \right) - \beta^2 \right] (MeV.cm) \tag{14}$$

where $\beta = v / c$ is the velocity of the particle, E is its energy, and z is its charge; ρ is the density of the material, N_A is the Avogadro number, and I is the mean excitation potential of the target.

3.4.2. Multiple and Compton scatterings

Scattering refers to a change of the direction of the particles.

Multiple Scattering

In the case of electrons and positrons, interactions with the atoms are due to electrostatic forces: the electron can then be scattered, meaning that its momentum is changing, either elastically and inelastically. The elastic scattering corresponds to a Coulomb interaction with the nucleus field screened by atomic electrons: incoming electrons are diffracted. The inelastic scattering occurs as a result of Coulomb interaction between incident electron and the atomic electrons. The inelastic scattering can lead to the excitation of an atom, and can involve many atoms of the solid: inelastic scattering is harmful since the energy lost heats the target.

Compton Scattering

The scattering of photons from charged particles refers to Compton scattering (Fig. 13). An incoming photon gives part of its energy to an atomic electron. The scattered photon, according to the Planck relationship, has a lower frequency and a longer wavelength. The wavelength change depends only on the angle of scattering for a given target. The electron that received the extra energy can go back to its ground state by emitting a new photon.
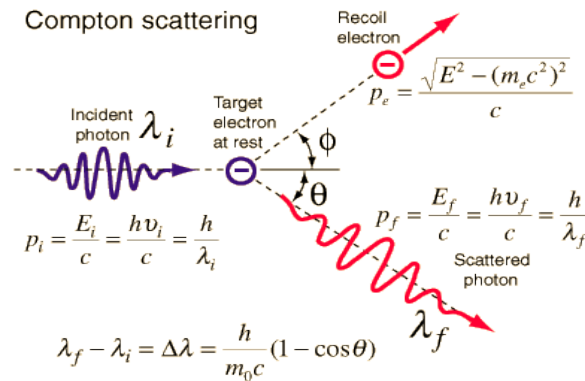

Figure 13: Compton scattering [19].

In these two processes, electrons and photons can be scattered with a wide range of angle and can even go backwards. It strongly depends on the atomic number of the material, and affects the electromagnetic cascade. The mean scattering angle for an electron of energy E_0 after a path x in the target is:

$$\theta \ (rd) \approx 21.2 \sqrt{\frac{1}{E_0} \frac{x}{X_0}} \tag{15}$$

There is also a transverse development of the shower due to multiple scattering of the electrons and Compton scattering of the photons, characterized by the Moliere radius r_m:

$$r_m = X_0 \frac{21.2}{E_C (MeV)} \tag{16}$$

3.4.3. Photoelectric effect

The photoelectric effect refers to the emission or ejection of an electron from an atom due to an incident photon. This process is more important than the creation pair for photon energy below 2 MeV.

The more intense light, the greater electron energy:

$$E_{e^-} = h\nu - E_{nlj} \tag{17}$$

where E_{nlj} is the bounding energy of the electron to the atom.

3.4.4. Positron annihilation

A positron created by a photon in the matter have a tendency to interact with atomic electrons since even if they are repelled by the magnetic force, they are attracted by the electric force. Then the exact opposite of the pair creation happens except that a positron annihilating with an electron gives two 511 keV photons emitted back-to-back.

4. Geant4 simulator

4.1. Basic description

Geant4 is resulting from a large international collaboration of physicist programmers and software engineers from Europe, USA, Japan and Canada [20]. Initially intended for high-energy physics experiment, it quickly became used by nuclear, accelerator, low-energy or medical physics community. The environment of Geant4 is C++. It is an improved version of the Geant3 simulation program which is in a FORTRAN based langage [21].
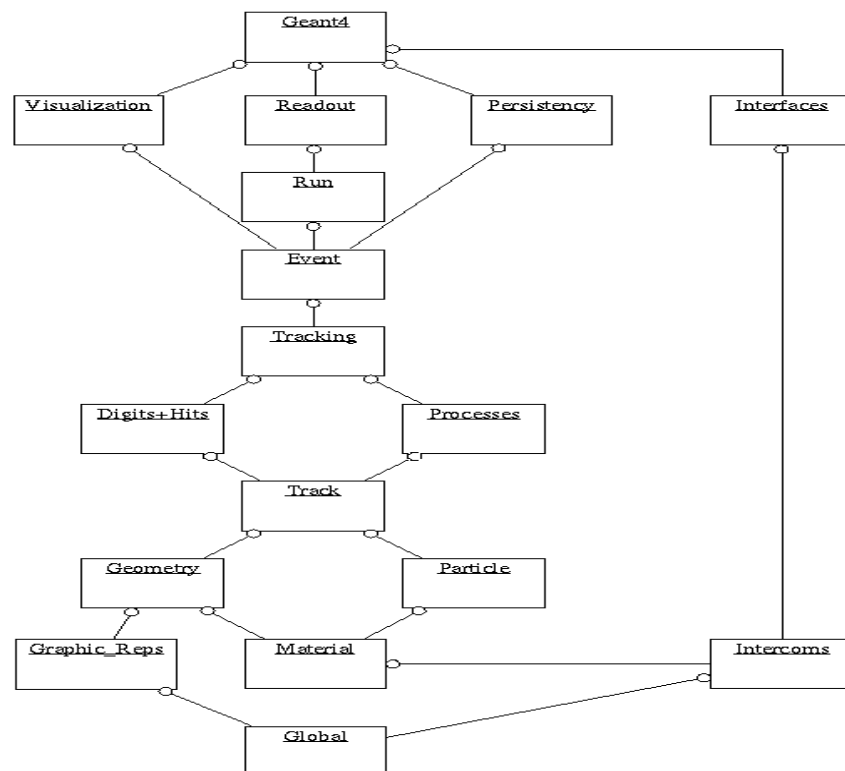

Figure 14: Geant4 class categories [20].

Geant4 is a powerful tool to get accurate simulations of particles going through matter, it deals with:

- the geometry of the system;
- the materials involved;
- the generation of primary events;
- the tracking of particles through materials and electromagnetic fields;
- the physics processes governing particle generation and interactions;
- the storage of events and tracks;
- the visualization of the detector and particle trajectories.

It is taking into account a large amount of physics models to handle interactions of particles with matter across a very wide energy range. The cross sections governing the physics processes are computed separately. Geant4 allows elaboration of very systems via small routines organized by class (Fig. 14).
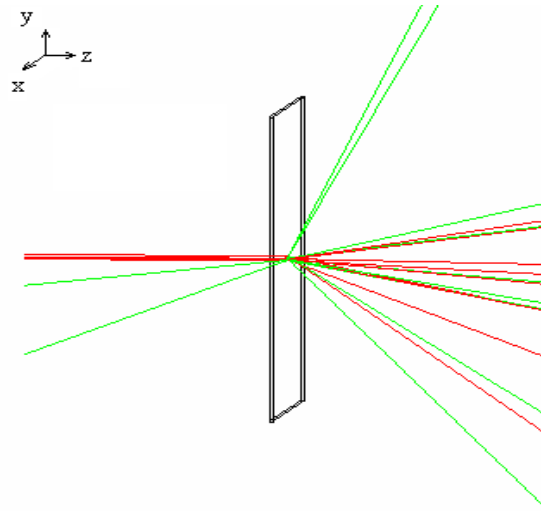
4.2. Positron beam generation

Figure 15: Electrons (Red) and photons (Green) at the exit of the target [2].

As described previously, high Z material are more efficient for the production of an electromagnetic shower. However, this is not the only criteria for choosing the target material: strength and resistance to shocks should be considered. Because of the side effects of the electromagnetic shower (multiple scattering, ionization, bremsstrahlung…) a good thermal conductivity and a high fusion point are advised to avoid target melting. Therefore, a tungsten foil is chosen: tungsten has Z=74 and a fusion point at 3695 K.
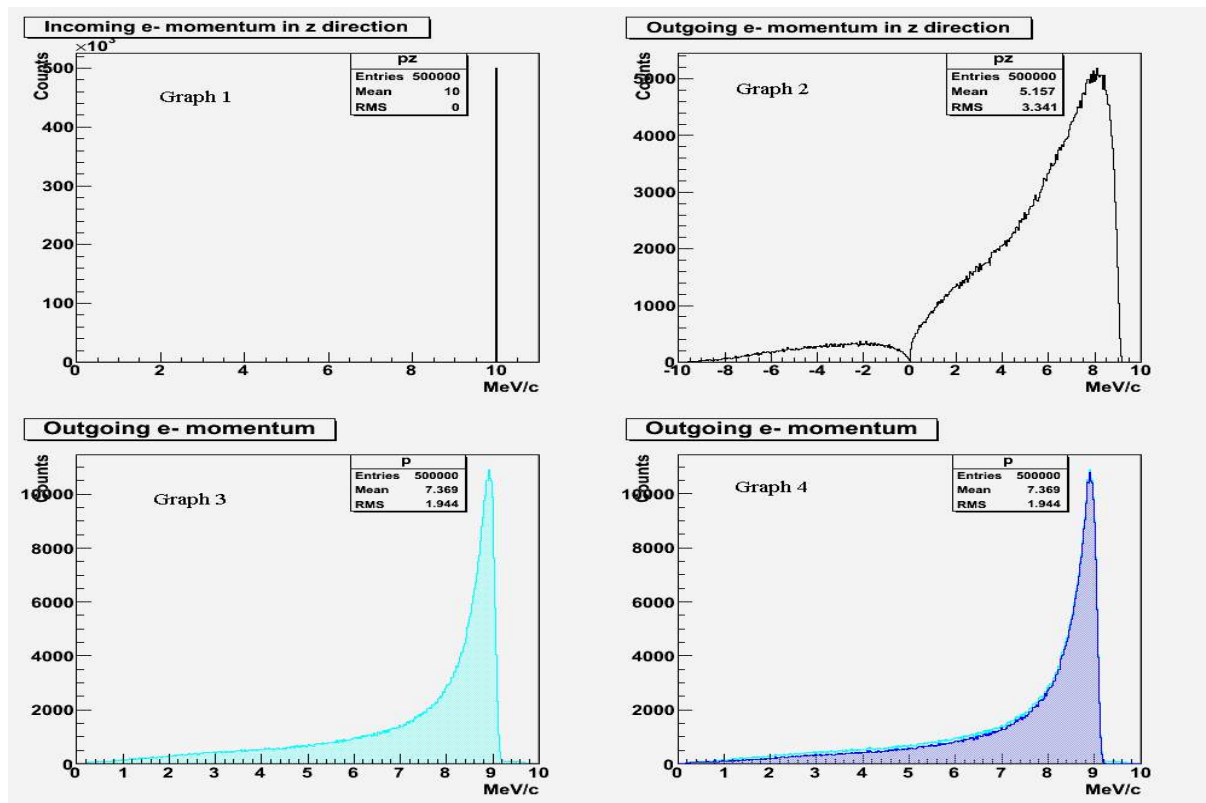

Figure 16: Momentum spectra of the incoming (graph 1) and outgoing electrons (graph 2, 3, 4).
outgoing electrons: z component of the momentum (graph 2); comparison of the momentum spectra of
downstream electrons (darker blue) with the global momentum spectra of outgoing electrons.

The other requirement is an electron beam. In the context of JLab, a 10 mA electron beam is envisaged. As a first step, a 10 MeV/c electron beam is considered, incident on a 0.5 mm thick target under a 90° angle; 500 000 events are generated. The beam direction defines the z axis which is having a Gaussian shape (0.5 mm full width at half maximum (FWHM)) in x and y (Fig. 17). The variation of the electron momentum is computed via Geant4. Figure 16 shows the main characteristics of the momentum of the electrons before and after passing through the target. The z component of outgoing electron momentum (graph n°2) shows that a subsequent part of the electrons are going backwards (7.5% of the total). Nevertheless the momentum profile of downstream electrons (graph n°4) is similar to the global profile. The mean energy lost by the electrons (graph n°3) is 2.6 MeV.
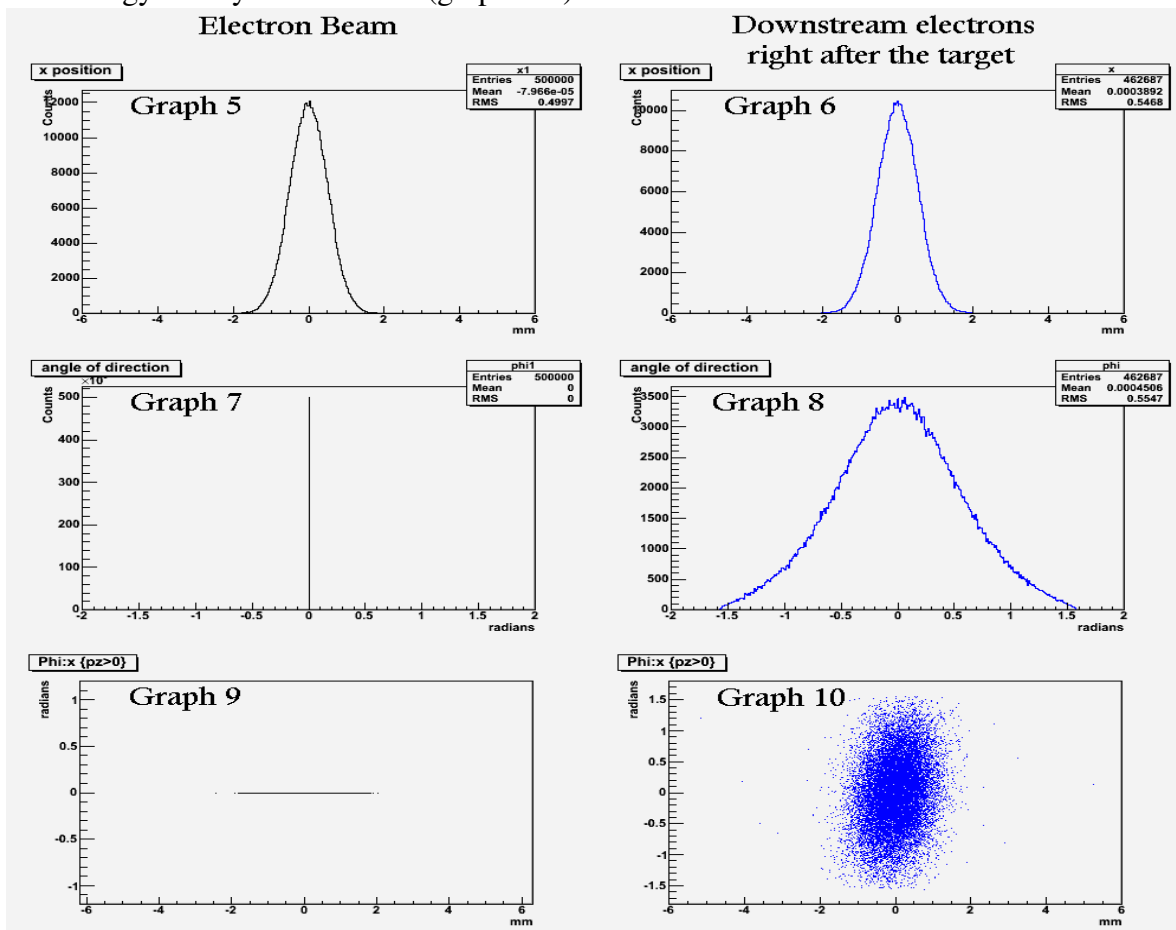

Figure 17: characteristics of the incoming (left side) and outgoing (right side) electron beam.
Particle position to the centre of the target on the x (graphs 5 and 6).
Electron direction angle relative to the x axis (graphs 7 and 8).
Phase space x axis (graphs 9 and 10)

The tracking of downstream electrons is an important concern of a positron source design. The next set of plots show the x phase space of electrons before (black) and after (blue) the target. The size of the beam at target is increasing from 0.5 mm to 0.54 mm (FWHM) right at the exit of the target (graph n°5). The effect on the direction angle (graph n°7 and n°8) is particularly striking: the electron beam shows, as requested, no angular dispersion while at the target exit there is a large spectrum; the most energetic particles keep the same direction while the low momentum electrons scatters to large angles. The electron phase space (graphs n°9

and n°10) shows the relation between the position of the particle and the angle of its direction with x (φ): this phase space after interaction has a characteristic ellipsoid shape which principal axis indicates the defocusing of the beam. The y phase space is similar.
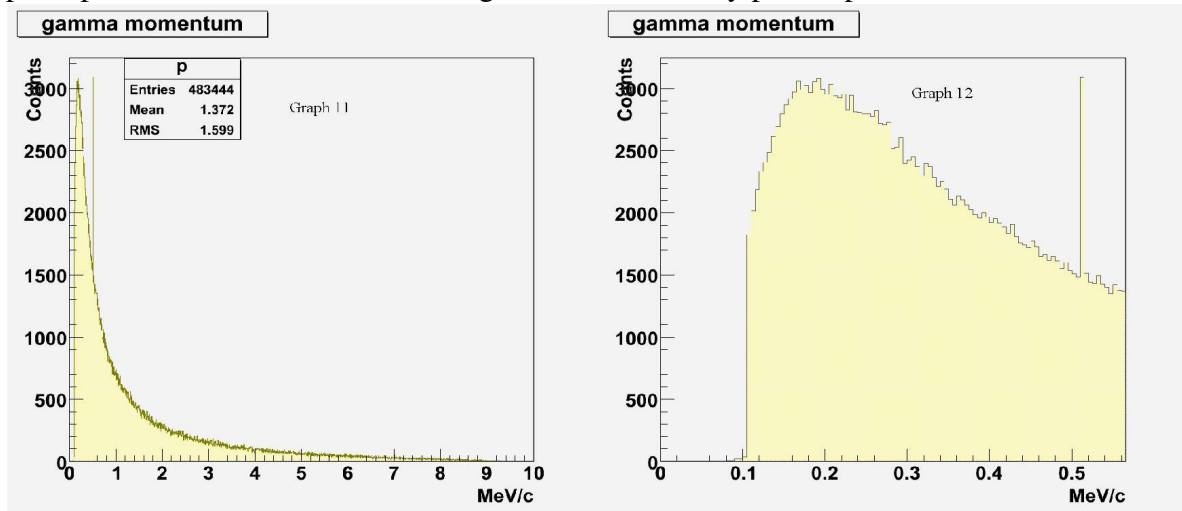

Figure 18: Photon energy spectrum at the target exit. The right panel is a zoom on the small energy region.

Of course, photons are also produced due to the electromagnetic shower. The energy spectrum of the photons shows a peak at 511keV due to e^-e^+ annihilation. Part of the very low energy photons are absorbed in the target, leading top a 100 keV threshold. About 1 photon per electron is produced in this example; the 1/E shape is characteristics of bremsstrahlung induced photons. Nevertheless, not all the photons escaped from the target; those photons are leading to the positrons of interest.
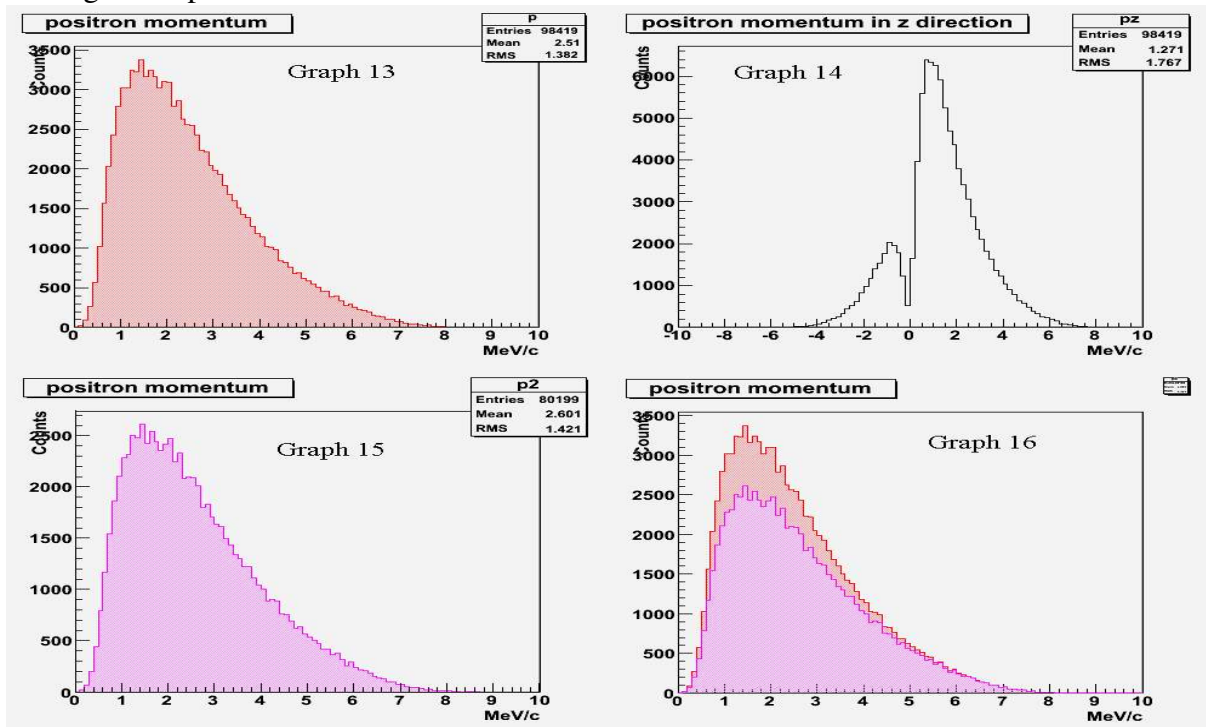

Figure 19: Momentum spectra of outgoing positrons (MeV/c): z component of the momentum (graph 14); comparison (graph 16) of the momentum spectra of downstream electrons (graph 15, purple) with the global momentum spectra of outgoing positrons (graph 13).

To get precise information 10^8 primary electrons are generated. Roughly the same number of photons is produced. Analyzing the positron momentum spectrum, one photon out of a thousand is producing a pair (graph 13). The mean positrons energy is 2.5 MeV with a maximum about 1.5 MeV. At this beam energy, downstream positrons represent 80% of the total produced flux. A precise view of the positron phase space in shown on Fig. 20. The positron spot in x (graph 17) and y (graph 18) right at the exit of the target is similar to the electron ones but a bit larger since the positrons are less energetic. As a consequence, the positron phase space is broader than the electrons ones.
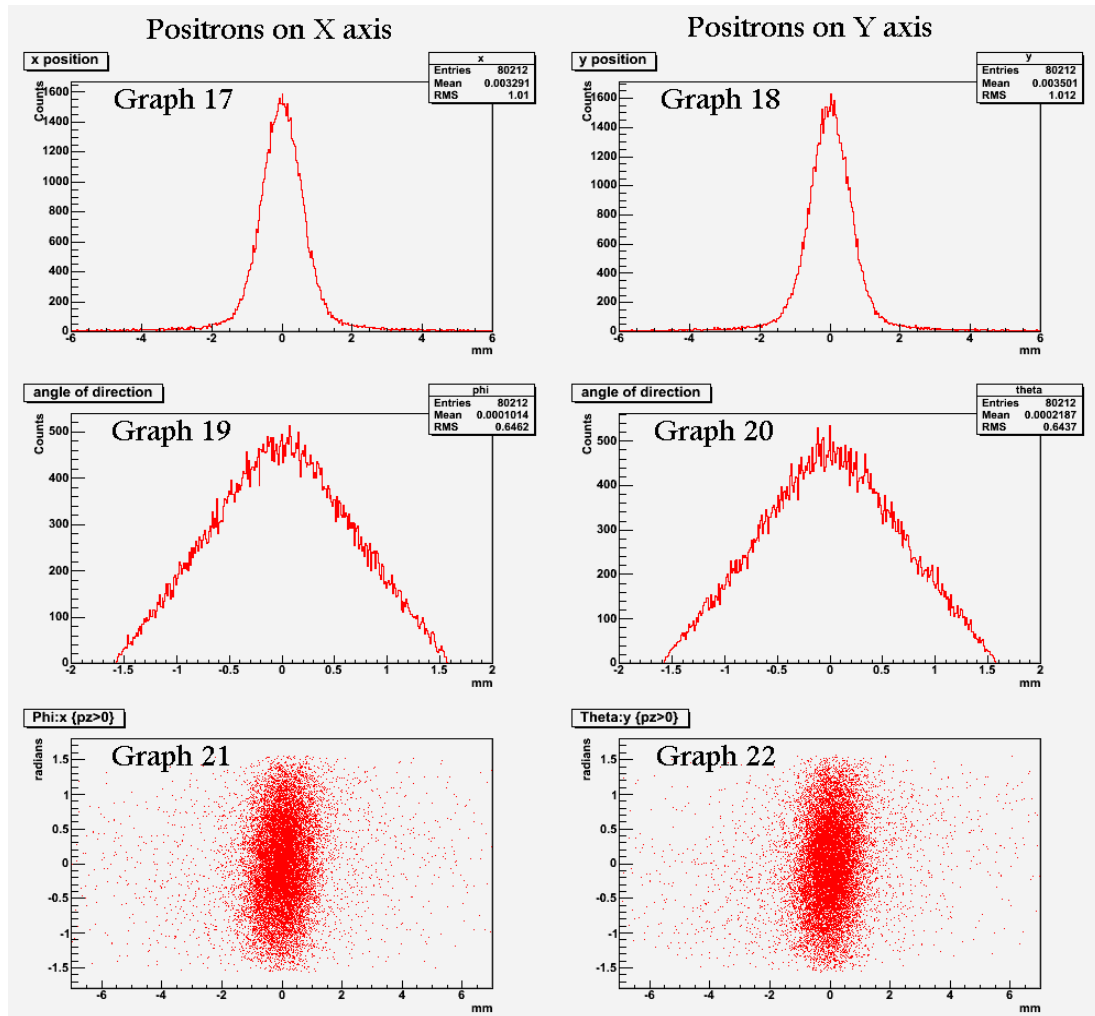

Figure 20: characteristics of the positrons tracks.
Particle positions to the centre of the target on the x (graph 17) and the y plane (graph 18).
Electron direction angle relative to the x axis (graphs 19 and 20).
Phase space x axis (graphs 21) and y axis (graph 22)

5. Results & discussions

Previously, the energy of the electron beam was 10 MeV, with an angle of incidence of 90° and the target was 0.5 mm thick. However, the influence of these parameters has to be studied in order to get optimized conditions for positrons production:

Four topics are discussed:
- The effect of the beam energy;
- The optimum target thickness;
- The heat load in the target;
- The incident angle of the beam at the target.

5.1. Influence of the beam energy

The ratio of positrons produced per electron sent is studied as a function of the beam energy. The thickness of the target is fixed at 0.5 mm and the incident angle of the beam is 90°. The number of positrons produced increases with energy, in a non-linear way (Fig. 21a). This is the consequence of the cross section of pair creation by a photon which is proportional to the logarithm of the photon energy. The photon energy is higher if the produced electron is more energetic.

The energy increase has also another positive effect, regarding the mean energy deposited by one incident electron and the particles it generated (Fig 21b). Indeed the higher beam energy, the less deposit. A closer look at simulation results reveals that it can be explained by the fact that the energy is deposited mostly by multi-scattering effect. The most energetic particles are less scattered and then less slowed down. The effect of multiple scattering at 100 MeV is decreasing compared to 5 MeV (about twice as less), while the number of photons produced by Bremsstrahlung is increasing by a factor 2.15.
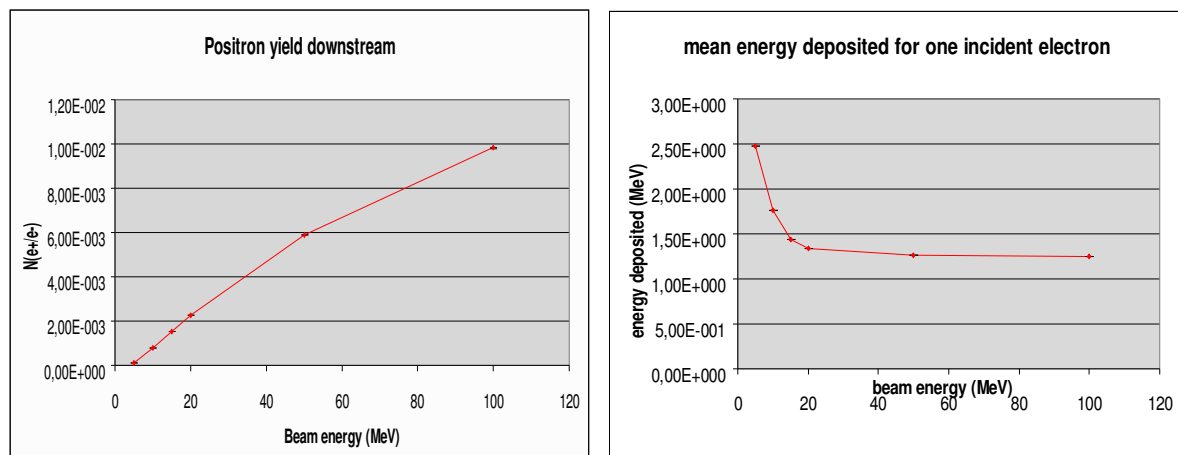

Figure 21a and b: evolution of the positron yield and the energy deposited as a function of the electrons energy in a 0.5mm tungsten foil.

The energy of the incoming beam has an additional effect on positron production. It concerns the positron positions, the number of positrons going downstream is more important, the next table (Fig. 24) shows that the ratios of the downstream positrons with the total positron yield

is increasing with energy. At 5 MeV, the ratio is reaching 70%, it means that 30% of the positrons will not take part to the positron beam whereas at 100 MeV 98% of the positrons are downstream. The cone of the electromagnetic shower taking into account all physic processes has an opening angle proportional to $\dfrac{1}{\sqrt{E_0}}$. The particles are less scattered to large angles with higher energies of the primary electrons E_0.

Aside from the positron yield, the beam energy has to be kept below the threshold for neutron activation of the target. That is 14.246 MeV for tungsten. At the Jefferson Lab, the injector of the Free Electron Laser is providing a 10 MeV electron beam.

5.2. Influence of the target thickness

Figure 22 reveals, before all, that the thickness has also an important role to play. The graphs show that the positron yield depends strongly on the target thickness.
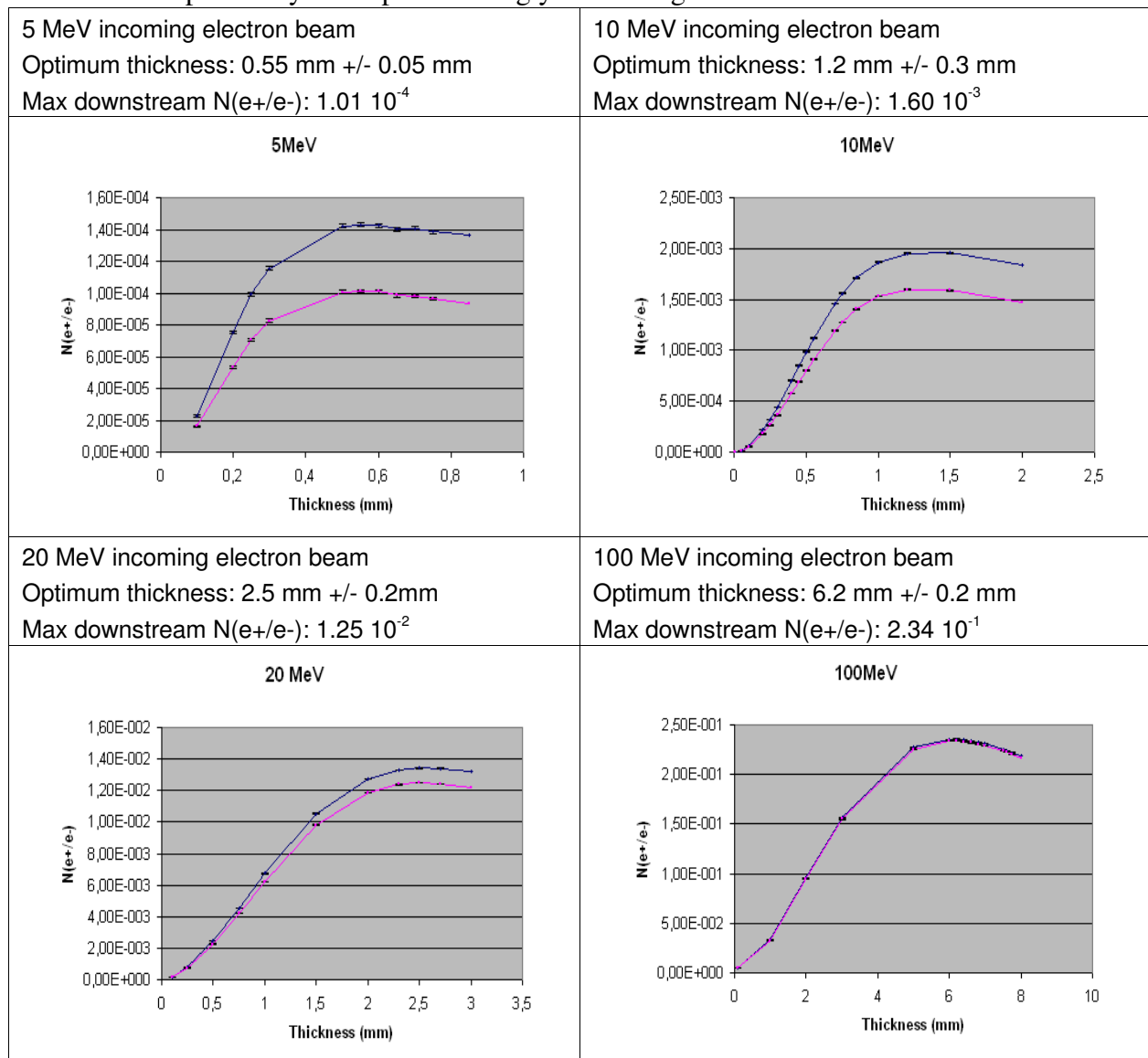
5 MeV incoming electron beam Optimum thickness: 0.55 mm +/- 0.05 mm Max downstream N(e+/e-): $1.01\ 10^{-4}$	10 MeV incoming electron beam Optimum thickness: 1.2 mm +/- 0.3 mm Max downstream N(e+/e-): $1.60\ 10^{-3}$
20 MeV incoming electron beam Optimum thickness: 2.5 mm +/- 0.2mm Max downstream N(e+/e-): $1.25\ 10^{-2}$	100 MeV incoming electron beam Optimum thickness: 6.2 mm +/- 0.2 mm Max downstream N(e+/e-): $2.34\ 10^{-1}$

Figure 22 : influence of the target thickness on the positron yield (Ne+/e-).
In blue the total positron yield and in pink the downstream positrons.

For 10 MeV, and a target of 0.5 mm, 8.02 x 10^{-4} positron is produced per electron while the positron yield is doubled for an optimum target thickness of 1.2 mm. The optimized target thickness increases with energy. According to the radiation length, for the electrons in a material, the longer the travel, the higher the particles production. However, particles created in the middle of a target that is too thick, are not able to come out. There is an optimum thickness that is large enough to enable the biggest electromagnetic shower to occur and thin enough to not stop the created particles. The optimum target thickness is the thickness corresponding to the highest positron yield without taking into account that the target could melt before this maximum positron production is reached. The positron yield as a function of the power deposited at the target has to be studied carefully.

5.3. Heating effects

When we normalize the positron production (Fig. 23), our results are compared with the JLab simulation (green), within the same context, similar results are obtained, however, the statistics is higher in our simulation (simulation with 10^7 electrons only at JLab against 10 times more in our case). The power deposit is more significant than the energy deposit because the time is taken into account. The optimum thickness is completely different. For a 10 MeV electron beam and a target thickness of 0.5 mm, the positron production is 8.02 e+/e-, while it is twice as much for the optimum thickness in the previous section. Taking into account the power deposited, an electron beam will produce 3.07 e+/e- per Watt deposited for a target thickness of 1.2 mm, and for 0.5 mm, the positron production per Watt is increasing by a factor of 1.5. To produce the same amount of positrons, the heat deposited is 50% higher for a target thickness of 1.2 than for 0.5 mm. The reason is that the power deposited in the target is not evolving as the same speed as the positron yield. The power deposited is given by:

$$P = \frac{E_{deposited}}{t} ,$$
(18)

$E_{deposited}$ is obtained by simulation for 10^8 primary electrons and particles generated, while the time:

$$t = \frac{Q}{I}$$
(19)

where I is the current of the beam (10mA) and Q is the charge 10^8 x 1.6 x 10^{-19} C. For a target thickness of 0.5 mm and a beam energy of 10 MeV, the power deposited in the target is:

$$P = \frac{1.76 \times 10^8 (MeV) \times 1.6 \times 10^{-13} \times 0.01 (A)}{10^8 \times 1.6 \times 10^{-19} (C)} = 1.76 \times 10^4 W .$$
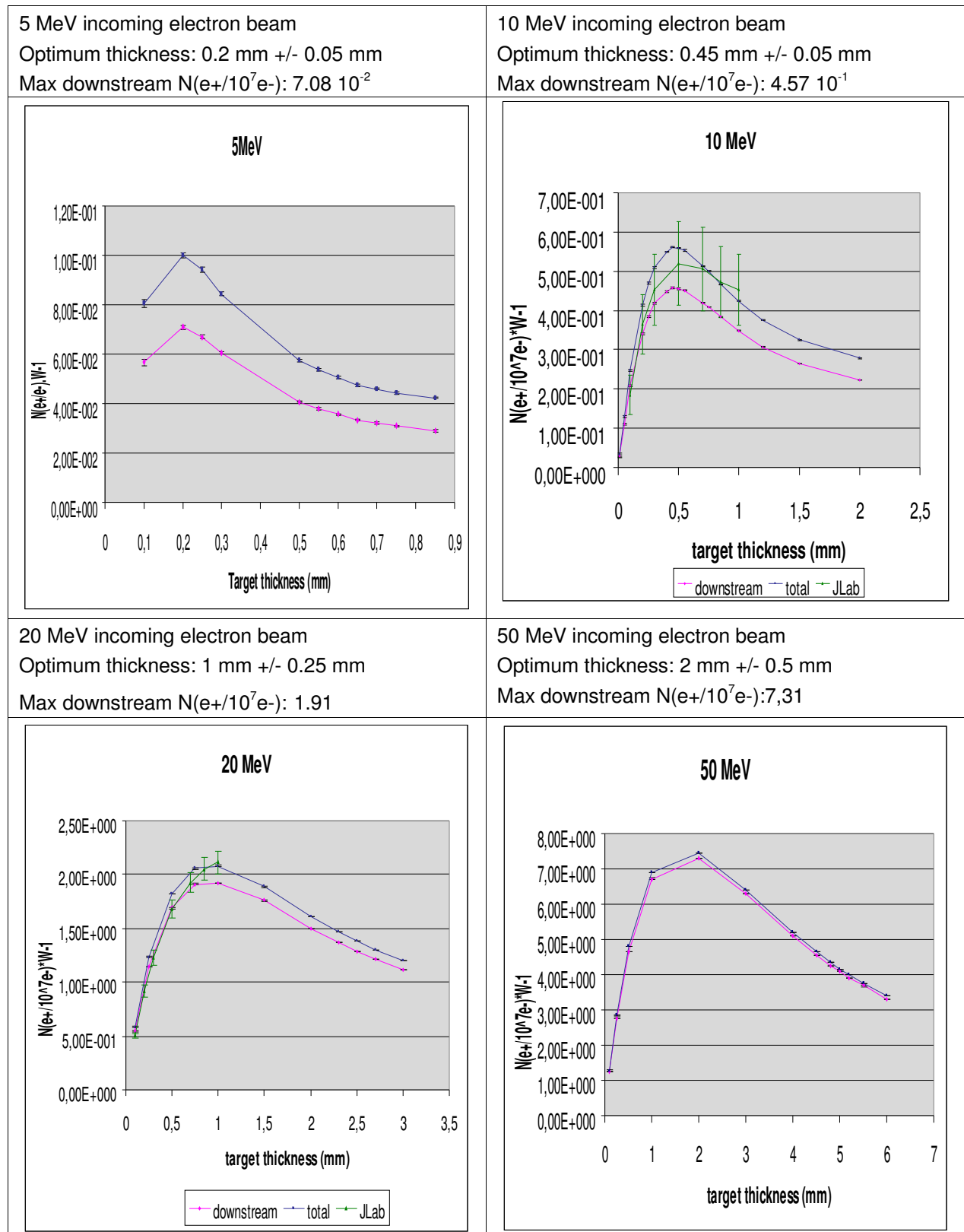
5 MeV incoming electron beam	10 MeV incoming electron beam
Optimum thickness: 0.2 mm +/- 0.05 mm	Optimum thickness: 0.45 mm +/- 0.05 mm
Max downstream $N(e+/10^7e-)$: $7.08\ 10^{-2}$	Max downstream $N(e+/10^7e-)$: $4.57\ 10^{-1}$

20 MeV incoming electron beam	50 MeV incoming electron beam
Optimum thickness: 1 mm +/- 0.25 mm	Optimum thickness: 2 mm +/- 0.5 mm
Max downstream $N(e+/10^7e-)$: 1.91	Max downstream $N(e+/10^7e-)$:7,31

Figure 23: influence of the target thickness on the power normalized positron yield $N(e+/10^7e-) \times W^1$

Figure 24 represents the power deposit (mW) per incident electron and shows a different shape from the positron yield (Fig. 22 - 10 MeV). The slope of the power deposited is steeper between 0.5 and 1.2 mm while for the positron production, it is between 0.2 and 0.85 mm.

Nevertheless, the heat losses are still an issue in the target. As mentioned in the positron beam generation part (section 4.2), the tungsten foil has a fusion point of 3695 K.
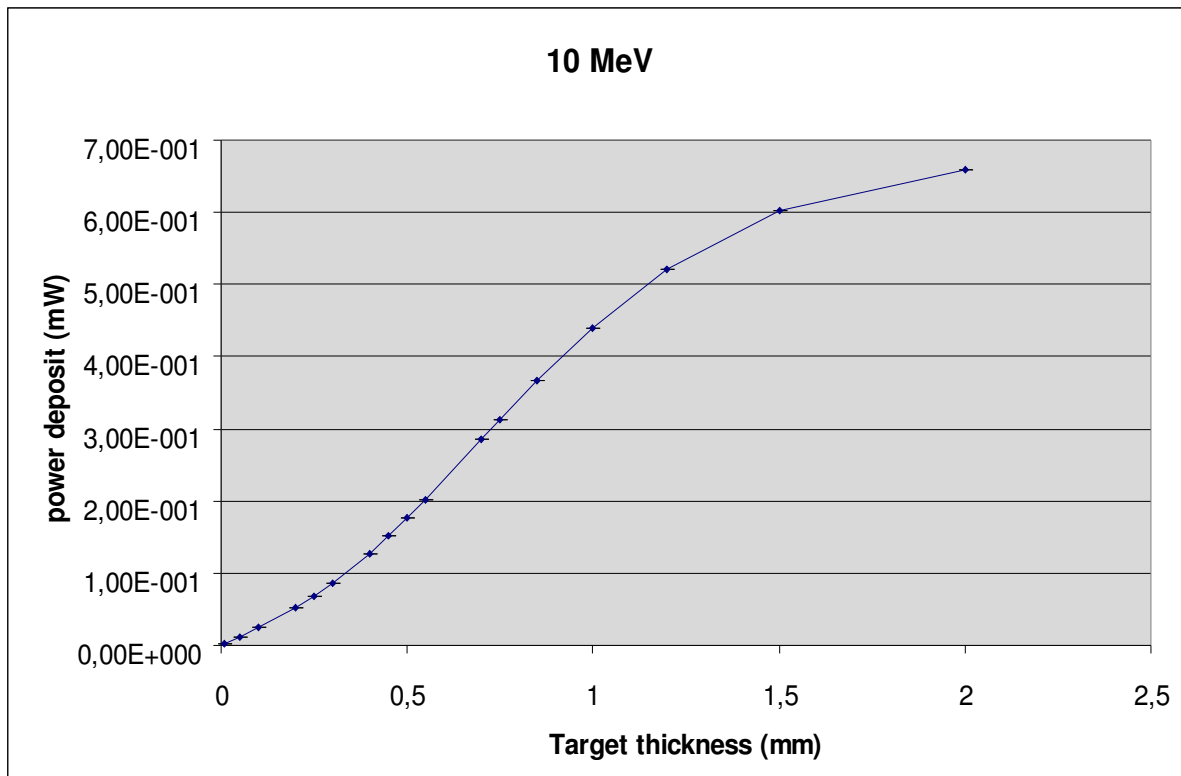

Figure 24: mean power deposit per electron as a function of the target thickness.

Unfortunately, even if the temperature of the target is kept below that point, the tungsten would still evaporate: 3100 K suffice to make the target loosing 10% of its mass in one hour or in 24 hours at 2700 K, according to the tables of Langmuir and Jones [20] on the evaporation rate of tungsten filaments under Joule effect. Some tests have been done with an electron gun intended to weld metal pieces, and a tungsten foil of 0.05 x 50 x 50 mm is able to resist to a power deposit (density flux) of 2 kW/cm^2, but 1 kW/cm^2 is considered as a limit in this study so that the tungsten foil doesn't melt.

According to our simulation, in the same conditions, the power deposited (1.18 kW) taking into account a spread of 0.5 mm (FWHM) of the beam (the spot area of the beam on the target is 0.79 mm^2 → 0.0079 cm^2). The density flux deposited is, then, 150 kW/cm^2

In our case a rotating target in order to change the spot that the beam is hitting could be a good mean to reduce the heat load.

5.4. Influence of the incidence angle

Another solution, which is not excluding the previous ones, is to choose a different incident angle of the beam on the tungsten foil [3]. The behaviour of the particles exiting the target for a beam with an incident angle of 3° is compared to 90° in this section.
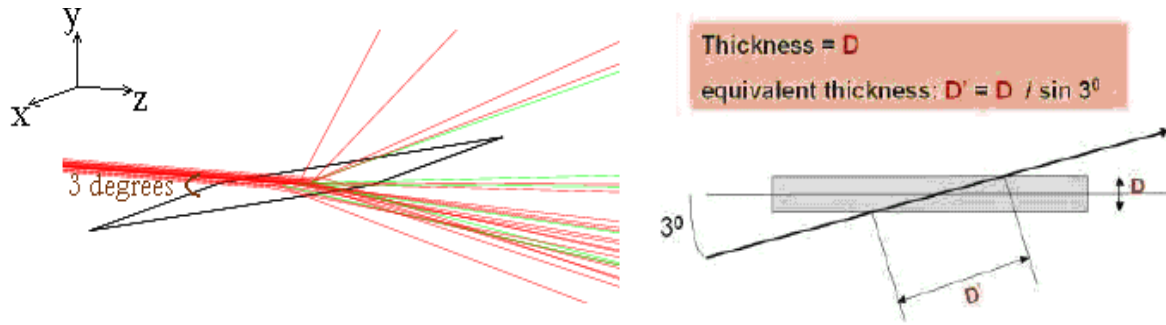
Figure 25: Electron beam with a 3° incident angle on the target.

Figure 26 compares the momentum of the downstream electrons for a beam hitting the target with an incidence of 90° (blue) and 3° (green). On the contrary of the 90° incidence spectrum, the electron momenta are extending till 10 MeV at 3°. The left panel graph shows that the amount of backward electrons is smaller at 3°.
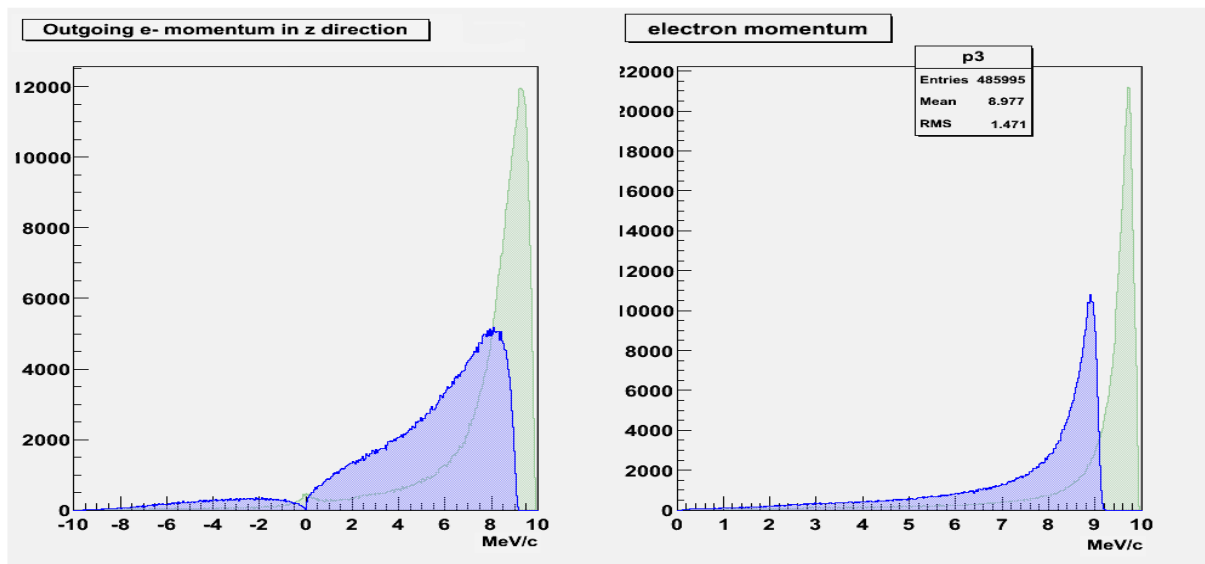

Figure 26: Energy spectrum comparison between an incidence of 90° (in blue) and 3° (in green).

The right panel shows that 2.8% (number of entries) of the electrons are going upstream at 3° against 7.5% at 90°. An electron is supposed to travel an equivalent distance through the target. In this example the electron is going across 0.5 mm but at 3° it does represent a target thickness of 26 μm. At 3°, the Molière radius of the electromagnetic shower (9 mm in Tungsten) is larger than the thickness of the target in the transverse plane of the beam. The particles of the electromagnetic shower are coming out of the target at 3° before than 90°.

The electrons are, then, less scattered. For example we compare the characteristics of the electrons 25 mm after the middle of the targets (along z plane), on the x plane, Graph 23, the positions of the 90° incidence electron (Blue) are wider than at 3° (Green). On the y plane (Graph 24), at 3° there are two peaks instead of one, the electrons are stopped by the target thickness along the z plane for y=0mm, the target is almost along the x0z plane.

The angles of direction relative to x axis(graph 25) and y axis (graph 26) are thinner at 3 degrees and as a result, the phase spaces are less extended (graphs 27, 28, 29 and 30).
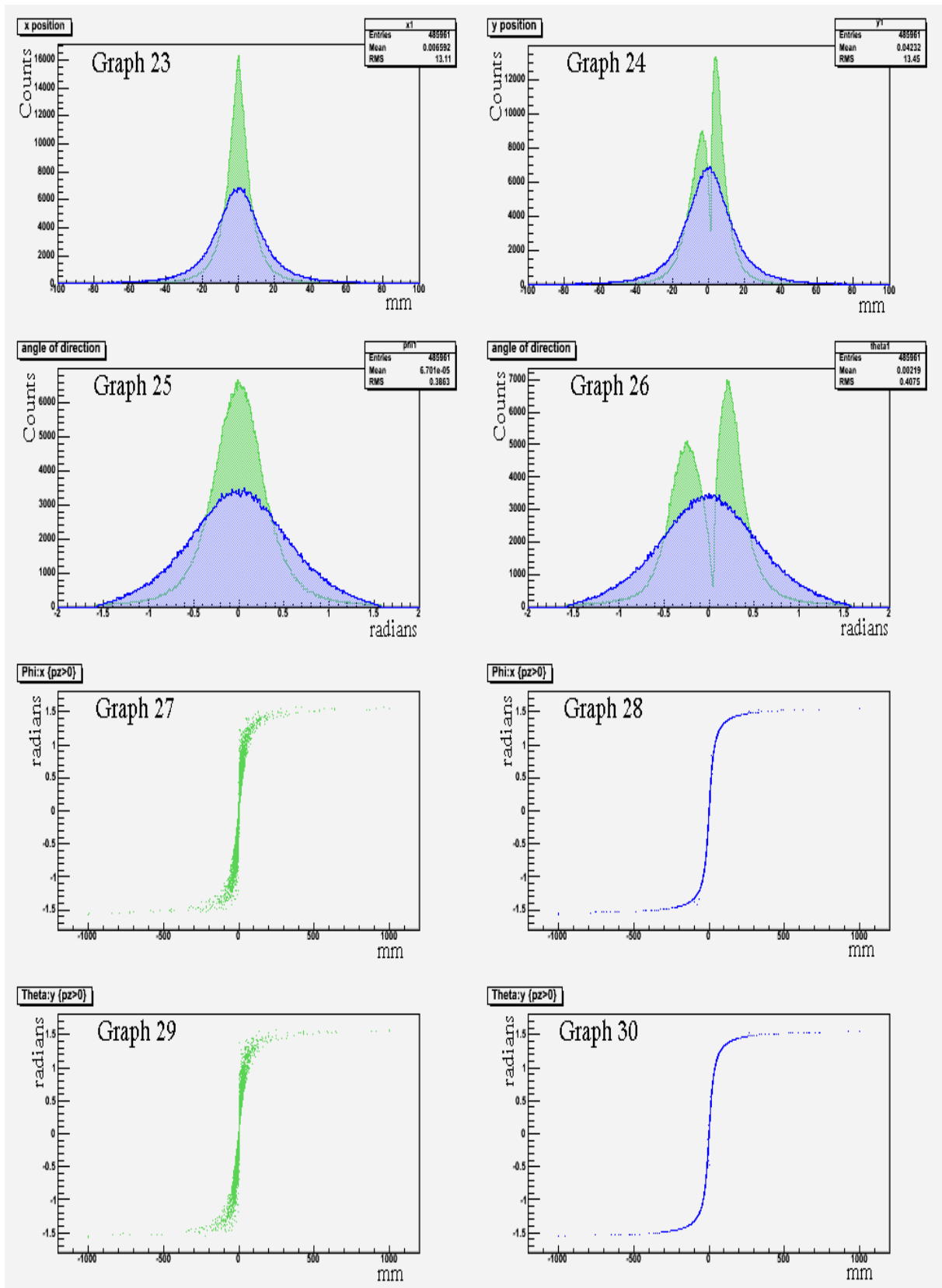
Figure 27: Comparison of the characteristic electron tracks between 3° (green) and 90° (blue) incident angle: particles positions of the centre at the target on the x (Graph 23) and y (Graph 24); Direction angles relative to the x axis (Graph 25) and y axis (Graph 26) of outgoing electrons; X phase space at 90° (Graph 27) and 3° (Graph 28); Y phase space at 90° (Graph 29) and 3° (Graph 30).

For the positrons (Fig. 28), the downstream positrons have slightly the same energy (2.601 MeV at 90° and 2.51 at 3°) but only 2/3 of positrons at 3° are produced compared to the positron yield at 90°.
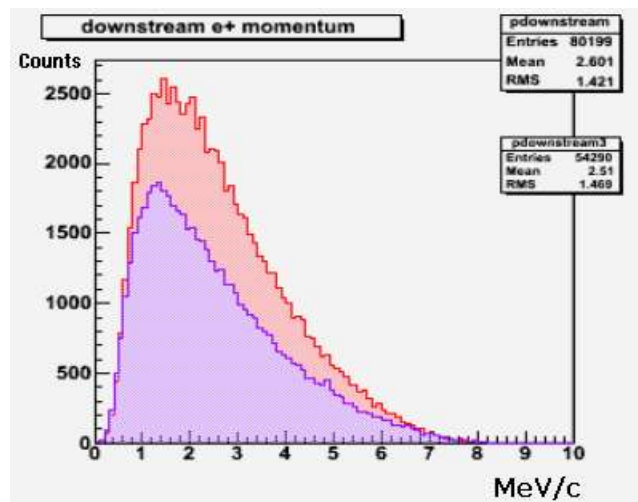

Figure 28: energy spectrum comparison between an incidence of 90 degrees (red) and 3 degrees (purple).

As a result of the change of the incident angle, the volume of the target is much lower: there is 20 times less material for a target of 26 μm thick than for a 0.5 mm thickness. Particles scatter less in the target and are ejected out of the material too quickly to produce a big electromagnetic shower. Figure 29 and 30 show that positrons evolve similarly to electrons.
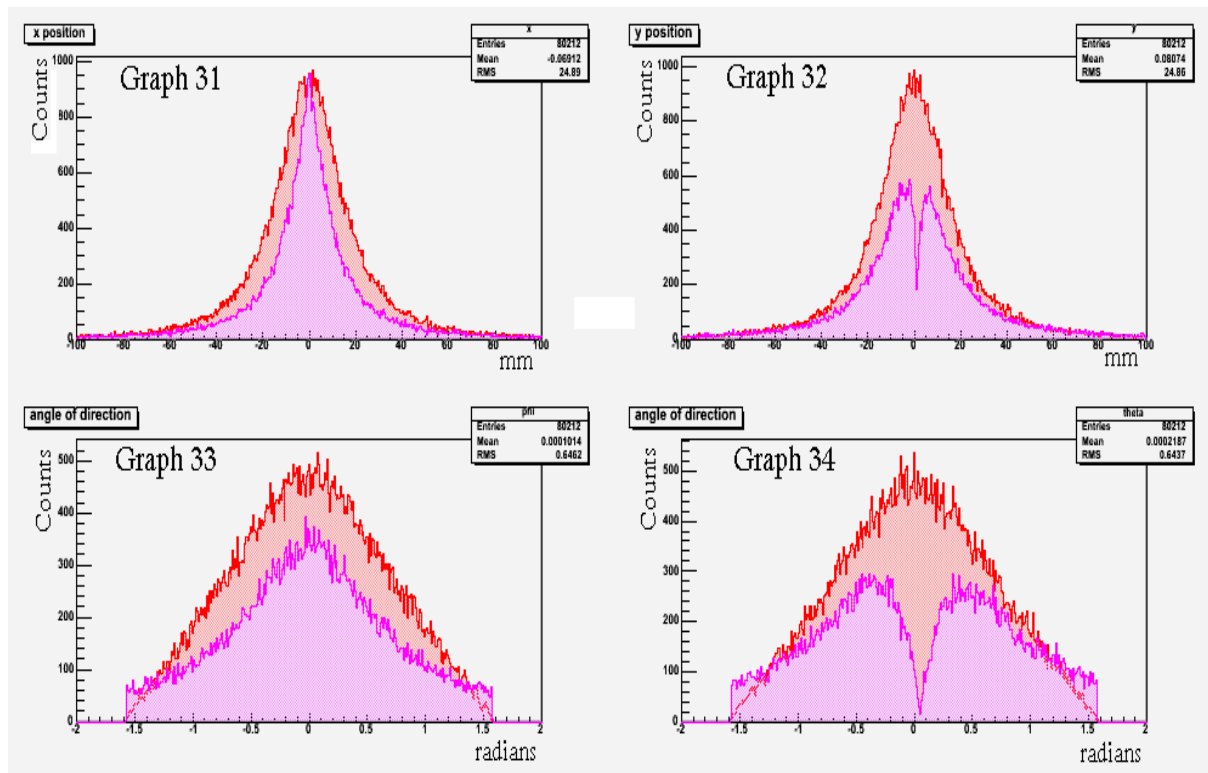

Figure 29: Comparison of the characteristic electron tracks between 3° (purple) and 90° of incident angle (red): Particles position to the centre at the target on x plane (Graph 31) and y plane (Graph 32). Direction angles relative to the x axis of outgoing positrons (Graph 33) and y plane (Graph 34).
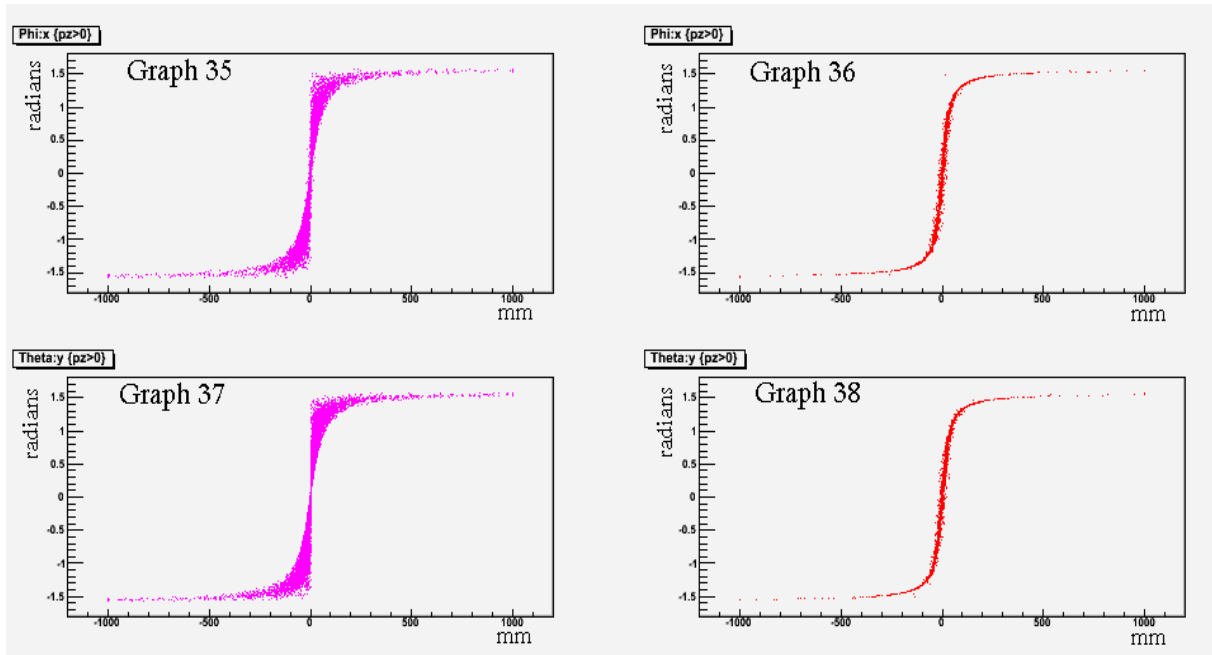
Figure 30: Comparison of the characteristic electron tracks between 3 ° (purple) and 90 ° of incident angle (red):
X phase space at 90 ° (Graph 35) and 3 ° (Graph 36);
Y phase space at 90 ° (Graph 37) and 3 ° (Graph 38).

However the change of incident angle of primary electrons on the target offers great benefits about the positron yield (Fig. 31), since the optimum thickness is not reached at 5 mm of
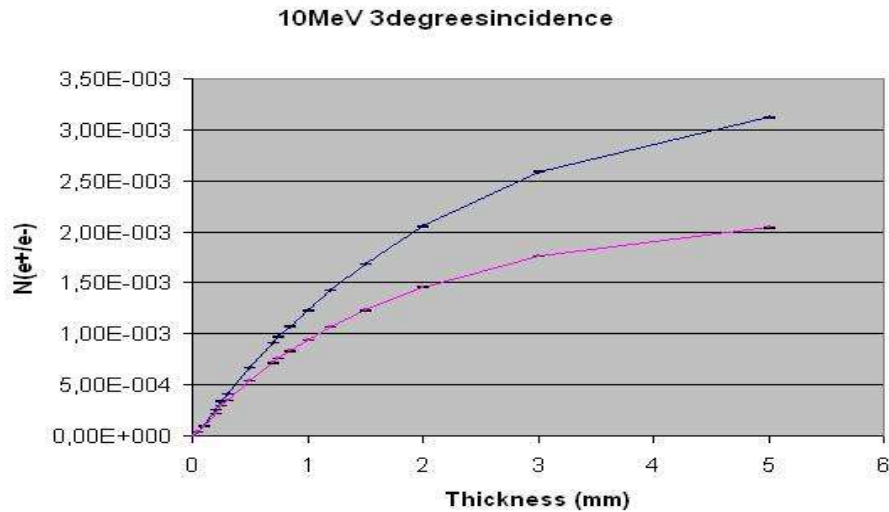

Figure 31: Positron production with 3 degrees incident beam.
Total positron yield (blue) and downstream positrons (pink).

equivalent target thickness. Comparing on Fig. 32a shows that a larger absolute positron yield can be obtained for a 3° incidence.

When normalized with the power deposit (Fig. 32b), the maximum positron produced is 1.7 positrons per 10^7 electrons and per Watt and almost 4 times less at 90°. The reason is that the energy deposited is several times lower at 3°.
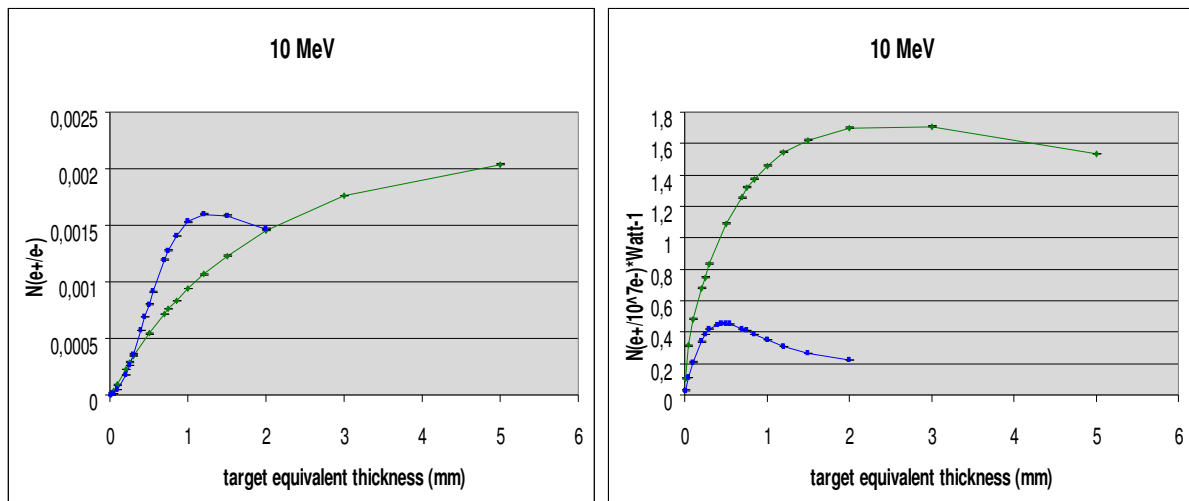
Figure 32 a and b: comparison of basic and normalized positron yield for an electron incident angles of 90 ° (blue) and 3 ° (green).

Multiple scattering effects which are the processes by which the more energy is deposited are 7 times lower at 3° and for Bremsstrahlung 10 times lower.
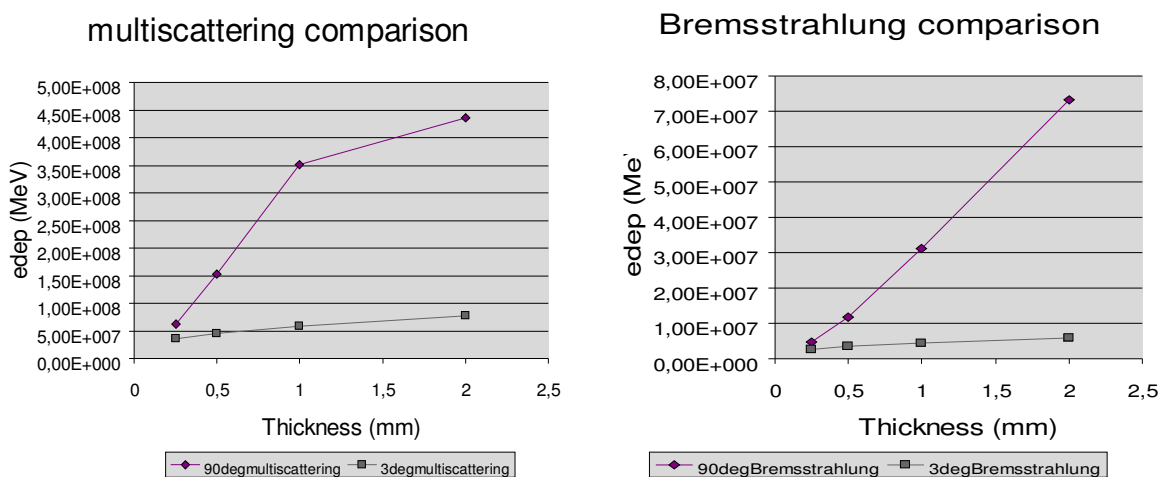

Figure 33 a and b: comparison of the energy deposited at 3 ° and 90 ° by multiple scattering and Bremsstrahlung.
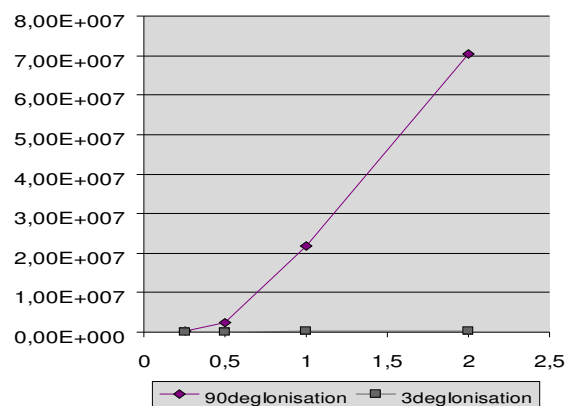

Figure 34: comparison of the energy deposited at 3 ° and 90 ° by ionisation.

The energy deposit by ionisation is negligible at 3° compared to 90°.

We can compare Figure 32b with the work that has been done in Saclay:
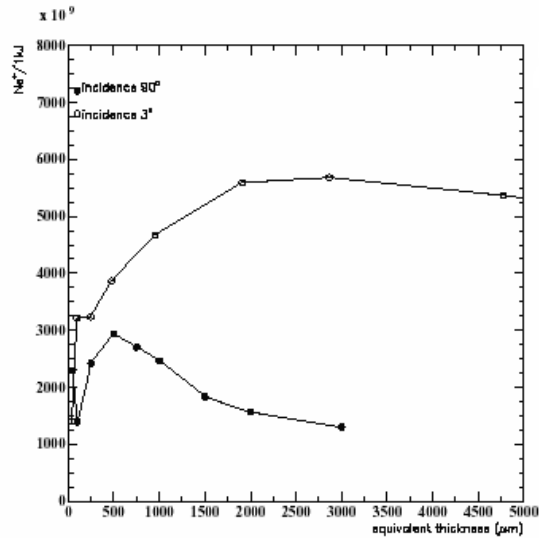

Figure 35: Produced positron rate downstream of the target for an electron intensity corresponding to a deposited power of 1 kW as a function of the equivalent target thickness crossed for 3 and 90 degree incidence angles and a beam energy of 10 MeV.[3]

It agrees on the optimum target thickness, but not on the shape of the positron yield under a target thickness of 0.25 mm, there is no reason to have a positron yield that is first decreasing then increasing and finally decrease again. For the amount of power deposited, Saclay finds a power deposit of 4.5 kW (4.4 kW in our case with the same conditions) for a 10 MeV and 1mA beam with an incident angle of 90° and 1 mm of target thickness. However at 3° according to Saclay, 1.75kW is deposited while our simulation only 600W.
This discrepancy is not yet understood, notice that Saclay simulations were performed with Geant3 and for 10^7 electrons.

Comparing with the test that has been done in Saclay, the power deposited in a 0.05 mm target thickness (1.05 kW) taking into account a spread of 0.5 mm (FWHM) of the beam (the spot area of the beam on the target is 15 mm² ➜ 0.15 cm²). The density flux deposited is, then, 7 kW/cm² (vs 150 kW/cm² at 90°) which is much closer to 1 kW/cm² advised by Saclay. The size of the beam spot on the target is here making all the difference

6. Conclusion & outlook

The particles characteristics have been studied, the position, the angle of direction and phase space are defined.

We have been studying the influence of several parameters of the electron beam and the tungsten target on the positron yield. We have seen that the amount of produced positrons increases with the energy of the beam. The target thickness can be optimized to get either the highest amount of positrons or the highest rate of positron per Watt deposited in the target.

The last parameter is the incident angle of the electron beam at the target. Comparing with 90°, the positron production turns out to be more efficient at 3°, more positrons can be produced with a smaller power deposit.

The rotation of the target should also be considered to limit the heat load in a small volume. Other systems may be used such as a cooling gas around the target filled with a cooling gas.

The simulations shows that 10^{-4} positron can be produced per electron, with a power deposit less than 1kW in the whole material. It represents a positron beam of 1 μA if the current of the electron beam is at 10mA.

The next step would be to be able to collect the positrons and focus them into a beam. The positrons have also to be separated from the electrons. A dipole is an easy way of doing such a separation but dispersive effects on the positrons that must be limited.

Two plans are considered:

-a solenoid focusing the positrons (as well as the electrons) right at the exit of the target.

-a triplet of quadrupoles focusing positrons and defocusing electrons in one plane and the opposite effect in the other plane. To make a first selection of particles, a collimator could be installed at the exit of the triplet of quadrupoles, a slit in the corresponding plane would let pass a major part of the positrons while a major part of the electrons wouldn't.

Then the electrons have to be dumped so that they don't deposit energy in devices that are sensitive to heat load. The energy deposit by the photons has to be studied as well.

Finally, in the case of using positrons for physics experiments, the positrons have to be injected in the ring to be accelerated or just focused into a beam in the case of a matter probe.

REFRENCES

[1] V. Strakhovenko, X. Artru, R. Chebab, M. Chevallier, Nucl. Inst. Meth. **A 547**, 320 (2005).

[2] S. Golge, Ph.D. Review, Jefferson Laboratory (2006).

[3] P. Perez, A. Rosowsky, Nucl. Inst. Meth. **A 545**, 20 (2005).

[4] D.P. Wells, A.W. Hunt, L. Tchelidze, J. Kumar, K. Smith, S. Thompson, F. Selim, J. Williams, J.F. Harmon, S. Maloy, A. Roy, Nucl. Inst. Meth. **A 562**, 688 (2006).

[5]   http://www.slac.stanford.edu/ .

[6]   http://www-linac.kek.jp/slowpos/ .

[7]   http://www-pat.llnl.gov/Research/Positrons/ .

[8] The 12 GeV Upgrade of CEBAF, Pre-Conceptual Design Report, Jefferson Laboratory (2004); http://www.jlab.org/12GeV/ .

[9] A.V. Belitsky, D. Müller, Nucl. Phys. **A 711**, 118c (2002).

[10] R. Krause-Rehberg, H.S. Leipner "Structure of imperfect solids" Universität Halle

[11] I. Procházka, Charles University, Prague   "Materials structure" Vol.8 Number 2 2001; http://www.xray.cz/ms/bul2001-2.htm

[12] http://www-pat.llnl.gov/Research/Positrons/PositronMaterials.html .

[13] http://www.aps.anl.gov/xfd/tech_bulletins/tb7/TB-7_AppenC.html .

[14] http://www-ucjf.troja.mff.cuni.cz/~dolejsi/fyzika_V/energy_loss_of_electrons_in_lead_m.gif .

[15] http://www.astro.psu.edu/users/niel/astro485/lectures/lecture08-overhead05.jpg .

[16] http://www.astro.wisc.edu/~bank/index.html .

[17] http://resources.yesican-science.ca/trek/radiation/final/index_em_matter.html .

[18] http://www-zeus.physik.uni-bonn.de/~brock/feynman/vtp_ws0506/chapter02/em_shower.jpg .

[19] http://cph-theory.persiangig.com/1191-english2.htm .

[20] http://geant4.web.cern.ch/geant4/UserDocumentation/Welcome/IntroductionToGeant4/html/introductionToGeant4.html#1 .

[21] GEANT 3.14, CERN Computer Newsletter **200**, 13 (1990).